DEM simulations of initial deposition of colloidal particles around non-woven membrane spacers

Florian Chaumeil[1], Martin Crapper[1]*

[1]*School of Engineering, the University of Edinburgh, Edinburgh EH9 3JL, United Kingdom*
**Corresponding Author:*

Dr Martin Crapper
School of Engineering
The University of Edinburgh
The King's Buildings
Edinburgh
EH9 3JL, UK
Tel +44 (0) 131 650 5727
Fax not available

Abstract

The modelling of the initial deposition on membrane spacers of colloidal size particles immersed in a liquid is investigated using the Discrete Element Method (DEM). The ability of this method to model surface interactions allows the modelling of particle agglomeration and deposition at the particle scale. The numerical model adopts a mechanistic approach to represent the forces involved in colloidal suspension by including near wall drag retardation, surface interaction and Brownian forces. The model is implemented using the commercially available DEM package EDEM 2.3®, so that results can be replicated in a standard and user-friendly framework. The effect of different spacer orientation with respect to feed direction is examined and results show that deposition of particles are increased around the spacer joints when feed orientation bisects the spacers' angle; when one of the spacer filaments is aligned with the feed inflow deposition occurs exclusively and uniformly on it. Simulation results demonstrate the validity of such method to describe the small-scale behaviour of micro-particles around spacers.

Keyword: Discrete Element Method; DEM; fouling; spacers; deposition; colloid; simulation

1 Introduction

Spiral-wound modules (SWM) are used in many types of filtration processes like desalination, water purification and food processing since their spiral type configuration offers high specific membrane area. However, they are restricted in their performance by concentration polarisation and fouling, like any membrane process. This fouling results in increased capital and operating costs, for example in the installation of redundant modules, the replacement of used modules and in filtration efficiency drop. The spiral

configuration also requires membrane spacers to keep each layer of the spiral separated and provide sufficient room for the water inflow.

Spacers play an important role in membrane systems [1]. They support and separate membrane sheets, or layers, in SWMs, which is why they are also found in electro-dialysis stacks. They can have beneficial effects on mass transfer, homogenizing and mixing behaviour, hence reducing fouling [3]. Spacers are usually composed of net of intrer-locking filaments as shown in Figure 1 or more rarely of extrusions of membrane surface [4]. Feed spacers can be designed for enhancing re-suspension of the rejected species to the bulk of the feed flow and thus lowering concentration polarization in spiral wound membrane modules. However, one adverse effect is that they induce pressure drop along the membrane module; this can lead to higher power consumption as illustrated by Da Costa et al [5], who showed that hydrodynamic angles (α, β), Figure 1, are critical parameters in designing spacer-filled membrane channels. Pressure drop is dominated by the drag force on spacer strands and Darcy-Weisbach friction like kinetic losses due to the flow direction changes [6].

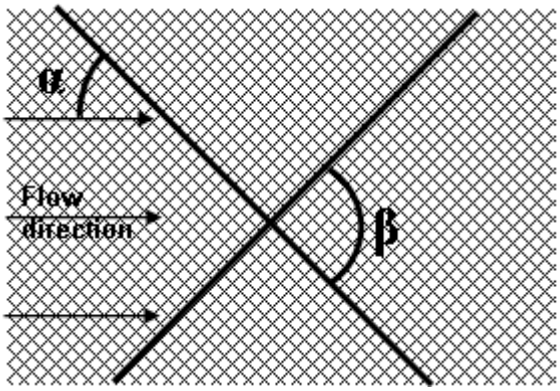

Figure 1: Sketch of net-type spacer's structure

In order to optimize the trade-off between enhanced mass transfer and increased cross-flow power consumption, CFD modelling [7, 8], [9], [10], [11, 12], [13], [14], [15, 16] has been used extensively. However, computational techniques have rarely been used to investigate the other issue of SWM, that is bio-fouling, arising from their extensive use in municipal water treatment plants and in industrial food processing. Spacer bio-fouling has been observed in industrial SWM autopsies, which are a laborious method and can be studied though a direct observation through membrane (DOTM) requiring expensive optical instrumentation. For this reason, numerical modelling can provide precious insight. Spacers provoked great interest and Vrouwenvelder et al [17] went as far as saying that "bio-fouling is a spacer and feed channel problem".

Bio-fouling occurs via the formation of a bio-film that is initiated by the adhesion of primary colonizing organisms like microbes and bacteria, whose adhesion is a controlled at first by long-range forces such as attractive Van-Der-Waals forces and repulsive electrostatic forces [18]. They form micro-colonies composed initially by organisms of same species. They later combine and form colonies and other types of bio-film structures composed of different microbial strains including algae, fungi and protozoa. These find energy and organic material (nutrient) for growth from dissolved feed-water organic material [19]

The critical flux of a membrane system is defined as the flux at which the relation between the trans-membrane pressure (TMP) and flux is no longer linear, due to matter deposition. Neal et al [20] used the DOTM technique to determine the effect of spacer orientation on this critical flux. They found that spacers significantly increase critical flux for a flow laden with 6.4μm latex beads. The degree of enhancement depended on spacer orientation, which means that spacer orientation has an effect on how particle deposit on the membrane. A similar observation technique was used by Vrouwenvelder et al [17] in order to observe the onset of bio-film formation on the spacer itself and showed that deposition initiates upstream of the spacer, in front of the filament junctions and to a lesser extent on the filament body after a long time. These results were later extended using the multi-physics package COMSOL and a cellular automata algorithm to numerically model the fluid dynamics and bio-fouling of feed channels [21]. It was shown that bio-fouling is a problem of initial deposition and bio-film growth and not a deposition effect due to filtration pressure. They confirmed that initial deposition occurs upstream of the spacers, but demonstrated that the biomass volume increase, that reduces the filtration efficiency, corresponds to microorganisms multiplication that accumulate mainly downstream of the spacer. Experimental work from Ngene [4] on a structured membrane, which is essentially a membrane with protrusions that play the same hydraulic role as SWM spacers, showed that there is initially a predominance of bio-film formation upstream of the structures, with a downstream formation of filamentous bio-film attached to the back of the structure at a later stage. Bio-film formation on the micro-obstacles was observed to be following a mechanism comparable to that on woven spacers [4].

Calculations made by Bacchin [22] et al suggested that critical flux depends strongly on particle size. For particles over 1μm, the shear-induced diffusion that lifts particles away from the membrane surface becomes significant and competes with the surface charge effects. Following this, a lower amount of foulant is observed with such particles, in comparison to the effects of bio-fouling, where extra-cellular polymeric substance (EPS) adherence and growth also contribute. In addition, for particulate fouling, there is a limited

mass of particles that can be deposited on the surface of the structures, after which there is equilibrium between the deposition and detachment of particles from the structure surface. However, the mechanisms of initial particle deposition strongly correlate with observations on primary bio-fouling [23]. It is therefore hypothesised that simulations of particulates as described in this work can predict initial deposition patterns which are applicable both to particulate fouling and to bio-fouling, meaning much can be learned about bio-fouling without the need to model the impact of EPS mediation and growth, which would be computationally expensive.

This work will describe a novel and easy method to address the issue of initial particulate and bio-film deposition. The later stages of microbial growth and colonization will not be considered, as it would require more extensive computational resources. Simulations will consider 2μm diameter size micro-particle (which is about the same size as common microbes such as *E. coli* [24]) around the joints of non-woven net type spacers, as those are the most commonly used in SWM. Simulations will only be considered at low inlet velocity, which correspond to lab scale setup rather than industrial application. This is because the effects of turbulence-particle interaction encountered at higher velocities remain an unresolved subject of ongoing research.

Particle scale modelling of agglomeration, cluster scouring and particle re-suspension as flocs can be simulated with DEM-CFD technique. It will be use to model the particle interactions with the spacers' surface and between themselves.

2 Definition of spacer geometry

Spacer geometry has been chosen to match the commercial range of spacers NALTEX-51 as this has already been subject to published studies, both experimental [5, 9], and computational [9], and has therefore a well defined geometry, with specifications readily available. Many studies [3, 11, 12, 25] use artificial, generalized dimensions in order to evaluate qualitatively spacers' mitigating effect on filtration. However, the present study seeks to evaluate the modelling method against previous results. Therefore, it has been chosen to model commonly cited configurations. There is a wide range of commercial spacers to choose from, but only a few particle deposition studies that poorly communicate the dimensions of their models. The Naltex series were the best documented ones at the time of this study, although no particle deposition study has been found with their exact geometry. It is however believed that deposition numbers and morphologies follow similar enough trends to be compared. Naltex basic geometry is shown in Figure.2.

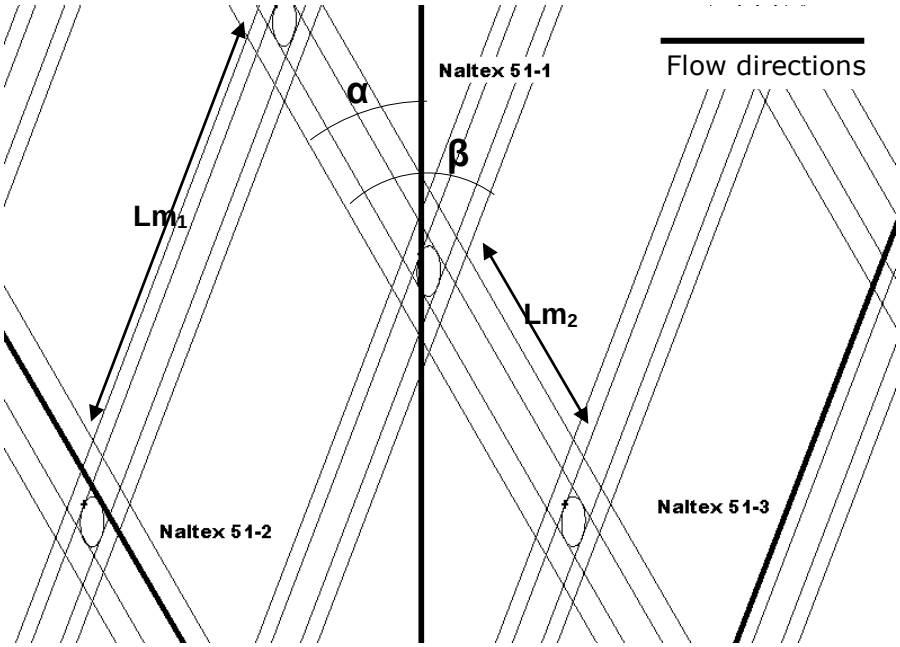

Figure.2: Naltex spacer parameters definition

Each product in the range is merely a rotation of the others by various angles, indicated by α and β in the figure. This fits the purpose of our work to model how the feed flow direction influences particle deposition on the spacer filaments.

Spacers parameters	Value
α	30°
β	51°
R_S (small filament radius)	0.25mm
R_B (big filament radius)	0.35mm
Lm_1	5.37mm
Lm_2	2.89mm
Filament overlap	0.03mm

Table.1: geometrical parameters of the Naltex-51 spacers

The three-dimensional model was built using GAMBIT 2.1® with dimensions provided in Table.1, and the fluid velocity field was computed with FLUENT 12.0® with a 1mm/s inlet velocity in order for the flow to remain laminar [13]. A particle-tracking model, implemented through the DEM software EDEM 2.3®, was used to simulate the particle deposition under the influence of both fluid drag and Van der Waals attraction, as described in the next section.

3 Force model

3.1 Definition of the mechanistic model

Both the shape of the computational domain and the inlet condition (flow rate, inlet velocity distribution) define the flow field inside the tube. The trajectories of immersed particles within the flow field are integrated for different particle sizes, particle concentrations and fluid flow rates, following the method described below.

The Lagrangian method determines the trajectory of each particle under the effect of colloidal and external forces, and the governing equation of particle transport is the stochastic Langevin equation, including particle Brownian motion. Particle trajectory and particle deposition are controlled by the combined influence of colloidal and hydrodynamic interactions, as is described by the force balance equation (1) [26]

$$m\frac{du_p}{dt} = F_D + F_G + F_L + F_{EDL} + F_{LVdW} + F_B$$

Eq. 1

Where m is the particle mass and u_p is the particle velocity vector. F_D is the fluid drag, F_G the force due to gravity, F_L the shear lift, F_{EDL} the electrostatic repulsion, F_{LVdW} the van der Waals attraction, and F_B the Brownian forces.

It is to be noted, however, that DEM is not commonly used to simulate processes involving very small finite particles, like colloids. The following paragraphs describe the models and equations required to model the flow of a dilute colloidal suspension.

3.2 Near the wall hydraulic retardation

In the vicinity of a channel wall, the displacement of the fluid between the particle and the wall becomes increasingly difficult because of the fluid between the particle and the wall needing to be accelerated (see Figure 3).

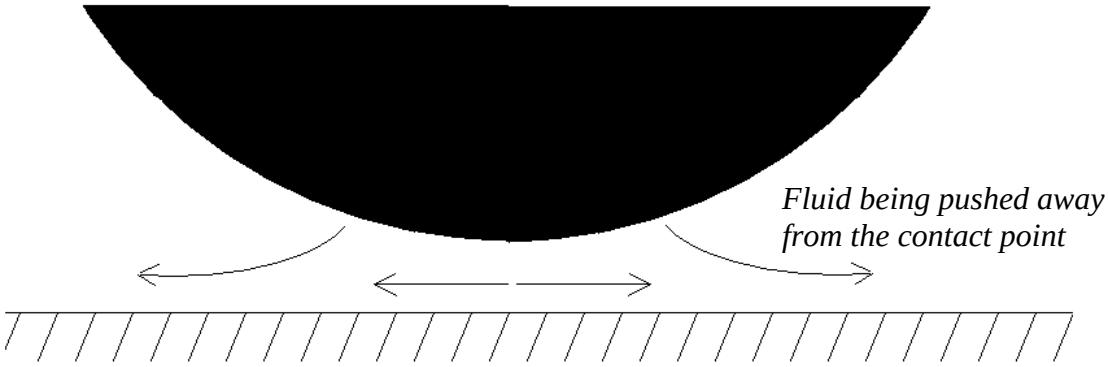

Figure 3: Fluid behaviour between a wall and an approaching particle

This causes the particle to bear an additional hydrodynamic drag over the Stokes drag on the particle. Hence, near a channel wall, particle motion is retarded due to the presence of the wall. Similarly, the presence of neighbouring particles causes the mutual retardation of the particles.

In order to consider this phenomenon we express the 3D-vector of the particle velocity in the wall's local reference frame as defined by the vector normal to the surface and two vectors normal to each other in the plane tangential to the surface.

Any motion of the particle relative to the wall can therefore be expressed as the sum of a velocity vector orthogonal to the wall with a velocity vector parallel to the wall. The following section explains how to use this decomposition to include the effect of the wall's presence.

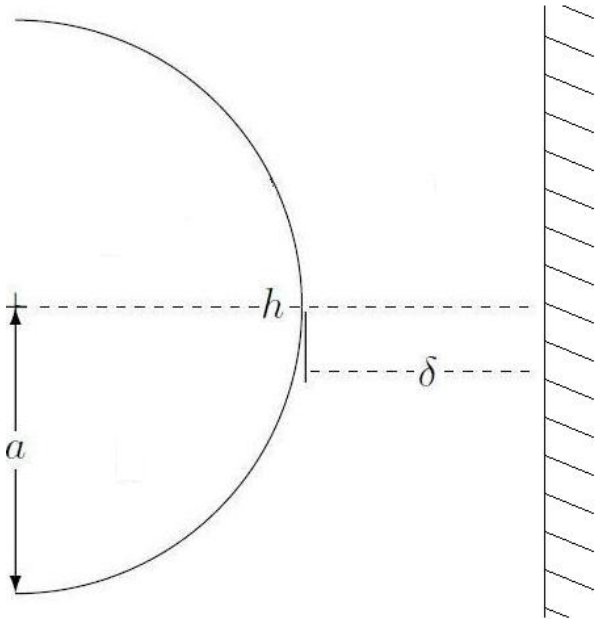

Figure 4: Fluid behaviour between a wall and an approaching particle

- Particle impinging Orthogonally on a rigid wall

The short-range hydrodynamic force, F, applied to a sphere with radius, R, can be described by the modified Stokes' equation[26]:

$$F_{D\perp} = F_1 + F_2 = -6\pi\mu.aV.\lambda_\perp + 6\pi\mu.aU.f_2$$

Eq. 2

In equation 2, the drag is composed of the sum of two terms:

- First term, F_1, corresponds to the case where the particle with velocity V normal to the wall moves in a zero velocity field and therefore experiences a drag in the opposite direction of its velocity.
- the second term, F_2 corresponds to the case of a motionless particle within a liquid flow field with velocity U at the location of the centre of the particle. The particle therefore experiences a drag in the same direction of the liquid velocity.

Equation 2 deviates from Stokes' law by the introduction of λ_t and f_2, correction factors that take into account the presence of a nearby wall. They are functions of the inter-surface separation distance, assuming a non-slip boundary condition applies to both the particle and solid surfaces. These factors tend to unity at a large enough distance from the wall.

For the situation in which the sphere radius is small compared to the separation distance, Lorentz[27] found that the resistance of the particle is greater than would be predicted by Stokes' law by a factor $\lambda_\perp$. Independently of the ratio of radius to distance, Brenner [28](1961) calculated the general analytical expression for $\lambda_\perp$, the first two terms of the Taylor expansion of $\lambda_\perp$ being the Lorentz formula. Nguyen and Evans (2007) derived the exact and approximate expressions for resistance coefficients of a motionless colloidal sphere approaching a solid surface. In order not to hinder computation efficiency, analytical retardation functions are accurately approximated by simpler equations. For a solid particle approaching a much larger solid surface with non-slip boundary conditions at low Reynolds numbers, the approximate solution is [29]:

$$f_2 = \frac{2.022+h/a}{0.626+h/a}$$

And

$$\lambda_{\perp} = \left[1+(a/h)^{p}\right]^{1/p}$$

With p=0.89

Eq. 3

h and a are as shown in Figure 4.

- Translational and rotational motion of a sphere parallel to a rigid wall

Considering Stokes' equations (Eq. 4), Goldman et al (1967) [30, 31] developed asymptotic solutions for the near-wall hydrodynamic forces when a particle flows past an obstacle:

$$\frac{1}{\mu}\overline{\nabla p} = \overline{\nabla^2 v}, \qquad \bar{\nabla}.\bar{v}=0$$

Eq. 4

For a non-rotating sphere near a plane in a quiescent fluid, Goldman et al computed the asymptotic drag function:

$$F_{D//}^{t*} \approx \frac{8}{15}\ln(\delta/a) - 0.9588$$

Eq. 5

where δ is as shown in Figure 4. Considering the linearity of Stokes' equations [31], Goldman et al superimposed the force induced by a linear shearing flow past an immobilized sphere near a rigid wall:

$$F_{D//}^{s} = 6\pi\mu a Sh\left(1+\frac{9}{16}\frac{a}{h}\right) \text{ with the fluid velocity } U_f = Sh.$$

Eq. 6

In the end the drag force acting on a sphere flowing closely along a wall is the sum of all contributions:

$$F_{D//} = 6\pi\mu a\left(UF_{D//}^{t*} + a\Omega F_{D//}^{r*} + Sh\left(1+\frac{9}{16}\frac{a}{h}\right)\right)$$

Eq. 7

3.3 Brownian motion and diffusion

For sub-micron sized particles, the local Stokes drag force must be corrected by a Cunningham factor [32], regardless of near the wall hydraulic retardation on the Stokes drag. The drag force expression is then given by:

$$F_D^{sub} = F_D^{ret} / C_C \text{ where } C_C = 1 + \frac{2\lambda}{d}\left(1.257 + 0.4e^{-0.55d/\lambda}\right)$$

Eq. 8

F_D^{ret} Is the usual drag force including the hydraulic retardation and λ is the molecular mean free path of the surrounding medium.

$$\lambda = \frac{\sqrt{mk_BT}}{\xi} \text{ [26] in a fluid and } \lambda = \frac{\mu}{\sqrt{2P\rho/\pi}} \text{ in a gas [33]}$$

Eq. 9

Where ξ is the drag or friction coefficient ($\xi = 6\pi.\mu.r_P$), k_B is the Boltzman constant and T is the temperature in Kelvin. Following the method used by Ounis et al. (1991) [32], the Brownian force components are independent white noise processes. At every time step, three independent Gaussian random numbers (G_i) of zero mean and unit variances are generated. These relate to the Brownian force (F_B), to be implemented in the momentum conservation equation (Eq. 1), by:

$$\overrightarrow{F_B} = \sum_{i=1}^{3} N_i \vec{e_i}$$

Eq. 10

Where N_i is the amplitude of the ith component of the Brownian force and has for its expression:

$$N_i = G_i\sqrt{\frac{\pi S}{\Delta t}} \text{ where } S = \frac{2k_BTf}{\pi}; \quad f = \frac{6\pi\mu r_p}{C_c} \text{ so } N_i = G_i\sqrt{\frac{6\pi\mu r_p.2k_BT}{\Delta t.C_C}}$$

Eq. 11

3.4 DLVO forces

The interaction between two charged solute particles is generally expressed by the DLVO potential, which comprises an attractive Lifshitz–Van der Waals (LVdW) and a repulsive electrostatic double layer (EDL) interaction[34].

The repulsive role of the electrical double layer and its correlation with particle roughness still being under investigation [26, 35], this work focuses on deposition under favourable conditions, meaning that simulations only consider attractive Van-Der-Waal interaction. Van-der-Waals force between two spherical surfaces immersed in a fluid medium is expressed as:

$$F_{lvdw} = \frac{32}{3} n^2 \lambda \pi^2 R \frac{b^3 a^3}{\left(\left((R+a)^2 - b^2\right)\left((R-a)^2 - b^2\right)\right)^2}$$

Eq. 12

(See Figure 5 for definitions of symbols.) For two spheres of same radius and very close to each other ($h << a$):

$$F_{lvdw} = \frac{Ha}{6h^2}$$

With $R = 2a + h$

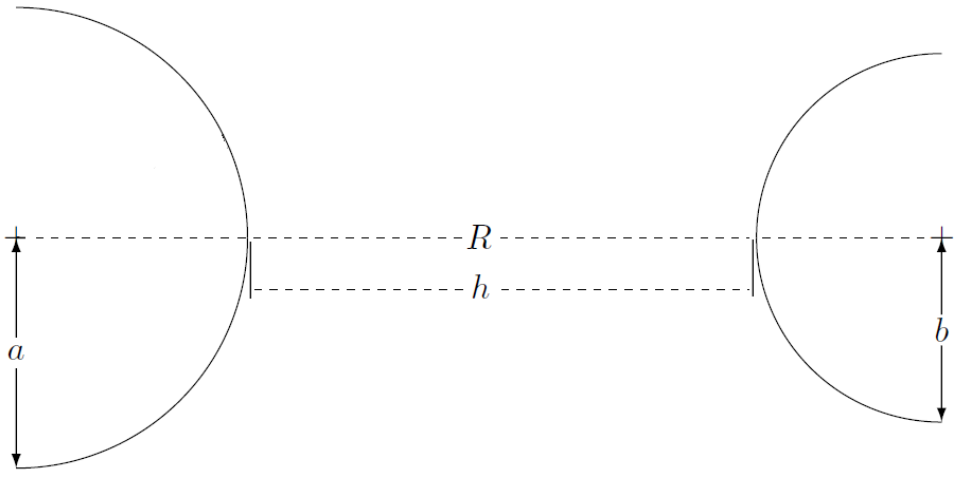

Figure 5: Interaction between two spherical particles

Magnetic retardation effects should also be included as a multiplying factor in the Van der Waals force expression [36]:

$$f_m = \frac{\lambda(\lambda + 22.24h)}{(\lambda + 11.12h)^2}$$

Eq. 13

The term λ is the characteristic wavelength of interaction, which is taken to be 10^{-7}. The simulation parameters common to all tested configurations are presented in Table 2.

Universal constant	Value
Boltzmann constant k_B	1.381e-23 J/K
Temperature T	300 K
characteristic wave length λ	1e-7 m
Hamaker constant $H = n^2 \lambda \pi^2$	1.5e-20 J
Water dynamic viscosity μ	1e-3 kg.s/m
Density of particle ρ_P	1e3 kg/m^3

Table 2: Simulation parameters

4 Model implementation

4.1 CFD method description

Due to the complexity of the spacer-filled channel to be modelled, computational fluid dynamics (CFD) was used to derive the flow velocity field, and an unstructured mesh was used (Figure 6).

The commercial software FLUENT 12.1 was used to solve the steady-state Navier-Stokes equations under laminar flow hydrodynamics. The mesh was created to ensure residual convergence and stability as well as independence of the solution.

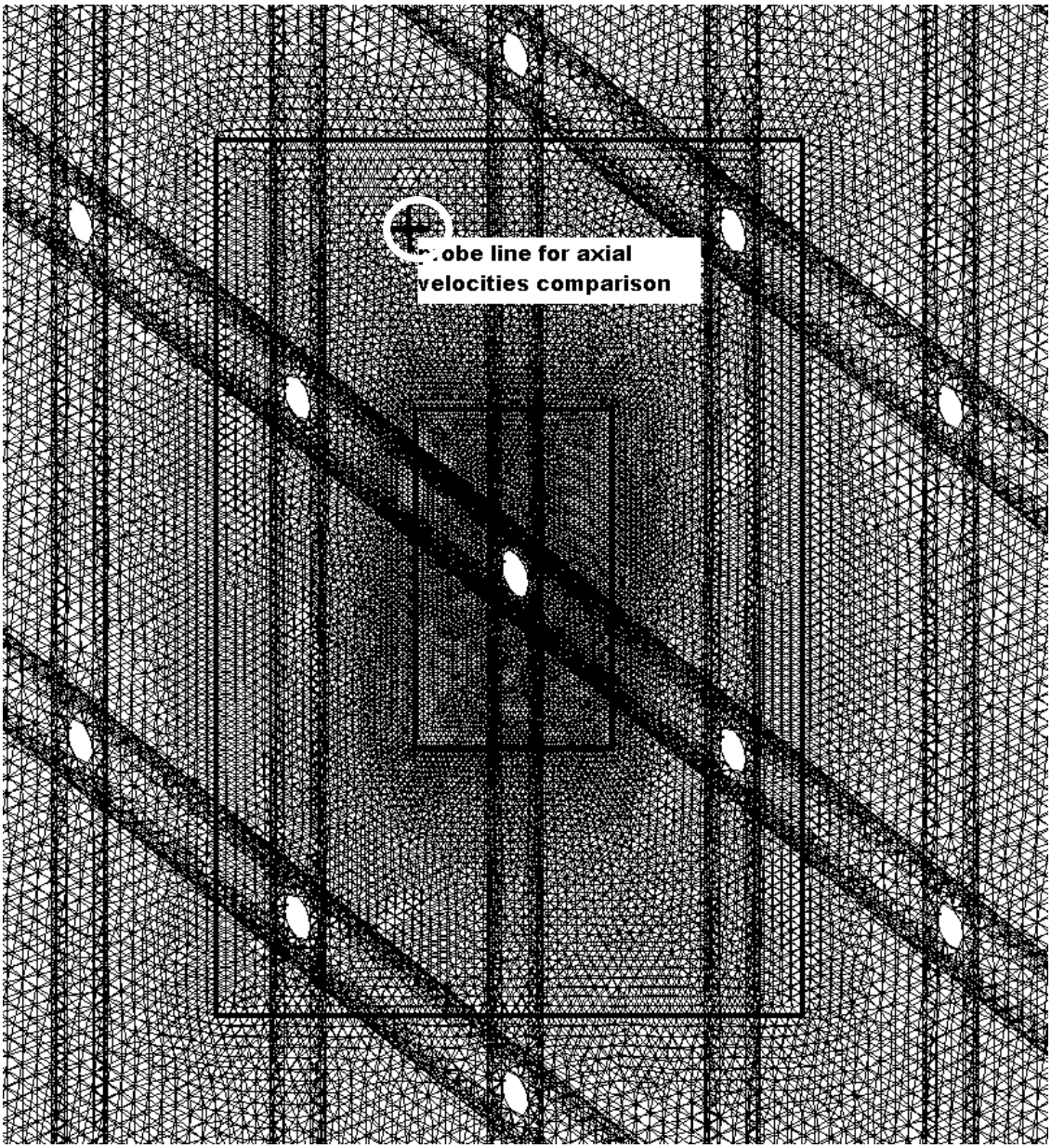

Figure.6: Unstructured mesh around spacer filaments joint

Boundary conditions for the model include no-slip boundaries at the spacers' wall surface, a no-slip condition at the membrane surface; permeate flow is considered slow enough to be neglected as [37], and a predefined inlet velocity of 1cm/s was used at the cell entry.

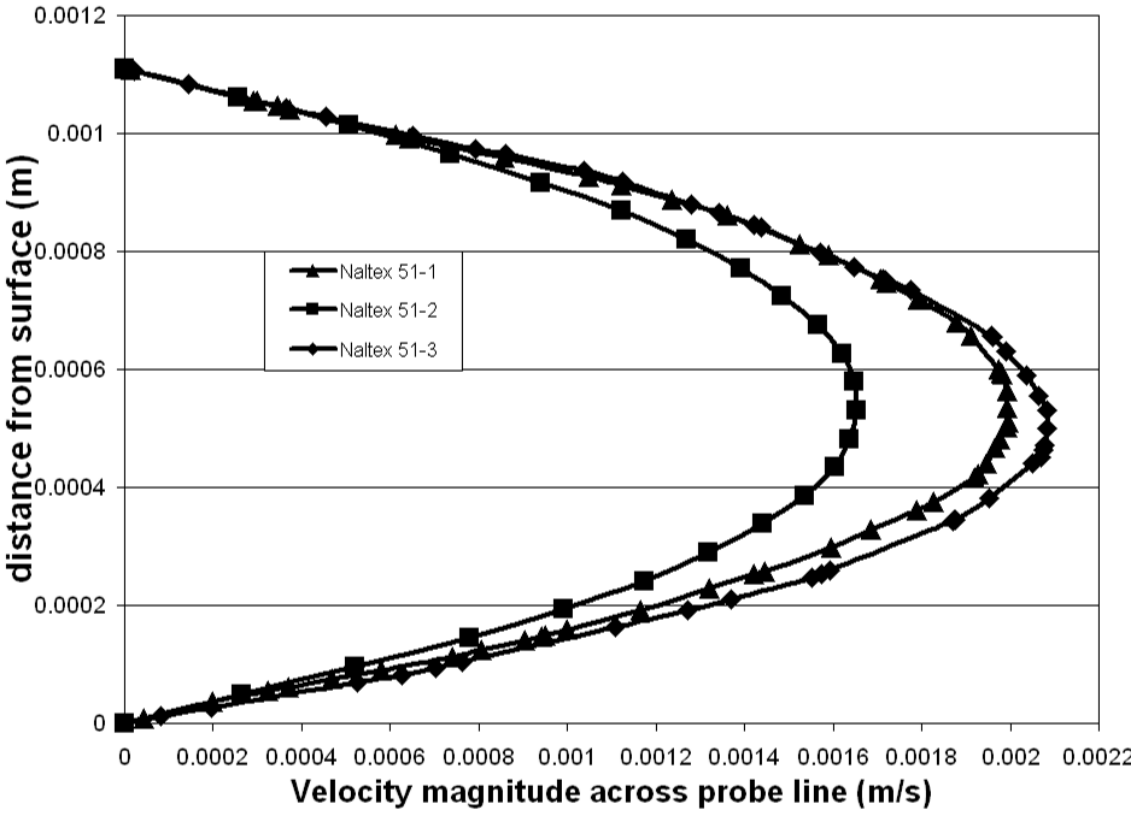

Figure.7: Axial fluid velocities comparison

Velocity magnitudes have been extracted from CFD results along a probe-line located at the centre of the spacer cells (Figure.6) in a similar manner to Karode and Kumar[9] (Figure.7). Velocity profiles appear to be close to parabolic, which is to be expected for a laminar flow between two plates. CFD results are also consistent with Wardeh and Morvan work [13], although their test feed channel geometry is slightly wider.

4.2 DEM implementation description

Mechanistic principles are implemented via the EDEM™ 2.3 software which allows coupling with CFD data, with the ability, via API programming, to add the required force models which are not standard to the software.

For each spacer configuration, particles were created within an inlet control window (Figure.8), which surrounds the spacer filaments. Following the limiting trajectory principle [38], particles injected further way from the wall would not contribute to the deposition process.

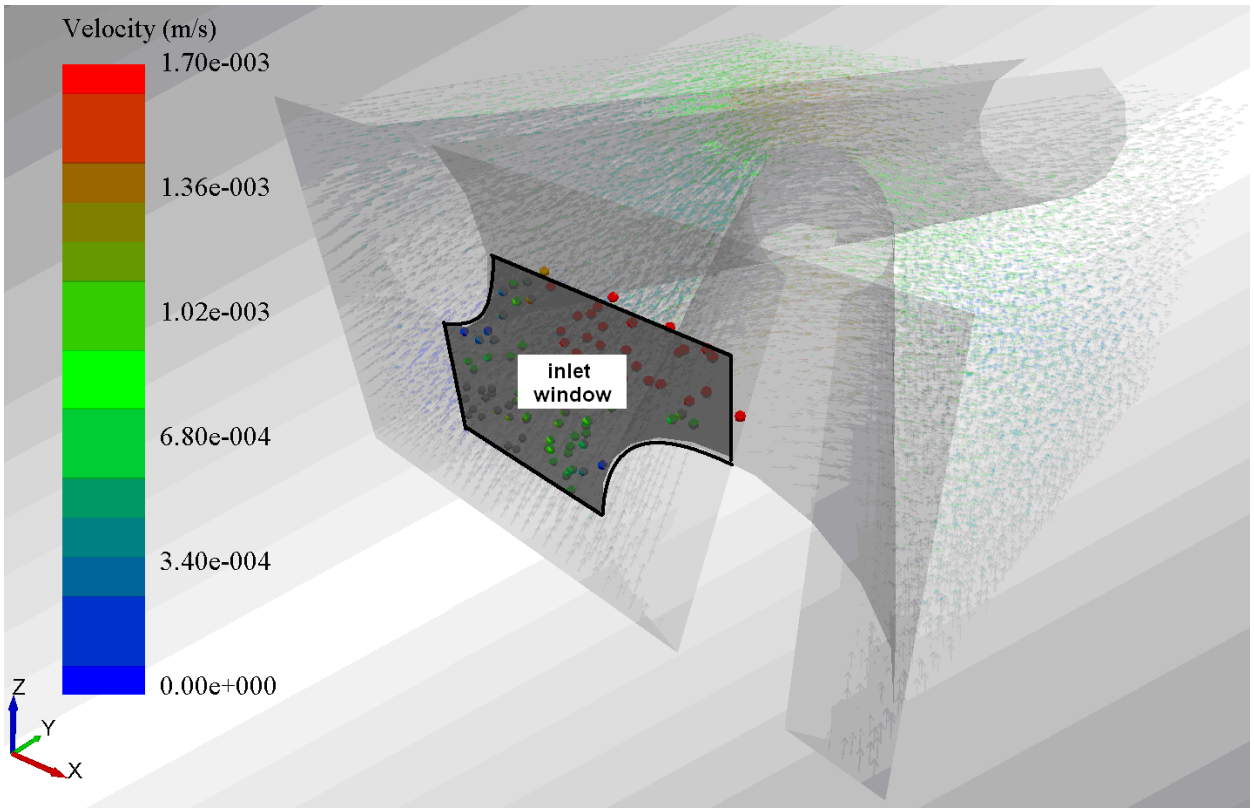

Figure.8: Particle inlet window

Particles were randomly created one by one following a uniform law over the control window surface. The particle creation rate was set to 10^5particles/s in order to allow a high enough concentration of particles in the computational volume and favour particle-to-particle collisions and cluster formation.

For each single simulation, the computation was left running until the suspended particles escaped entirely, on a 3GHz Core2 Quad CPU desktop computer with 3GB RAM, it took 6.5 days to run each of the three simulations. Once each simulation finished, only deposited particles remained in the computational domain, which provided a way to quantify the amount of deposited particle for each configuration.

5 Results and discussion

The number of particles deposited in each Naltex 51 spacer configuration obtained from the simulations is given in Figure.9. Results display the number of particles deposited in function of the axial distance from the spacer join, in the direction of the inlet flow.

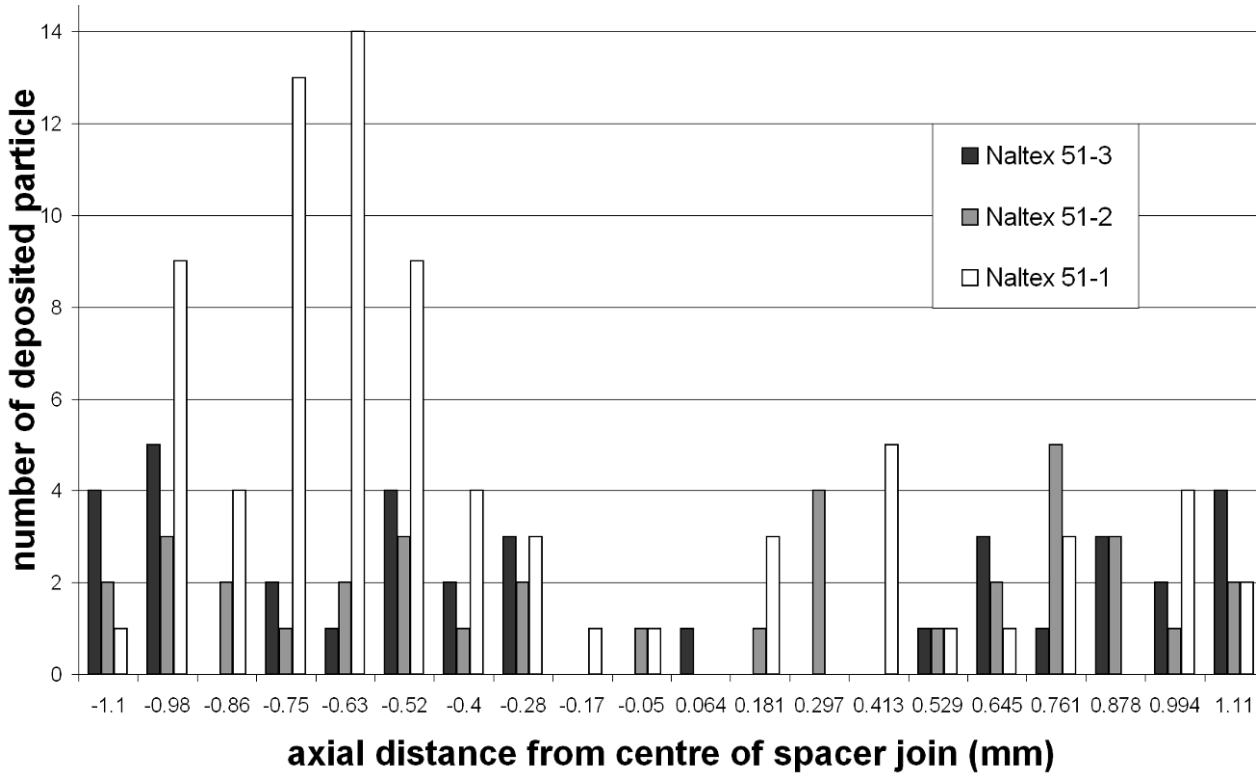

Figure.9: Number of deposited particles for each configuration

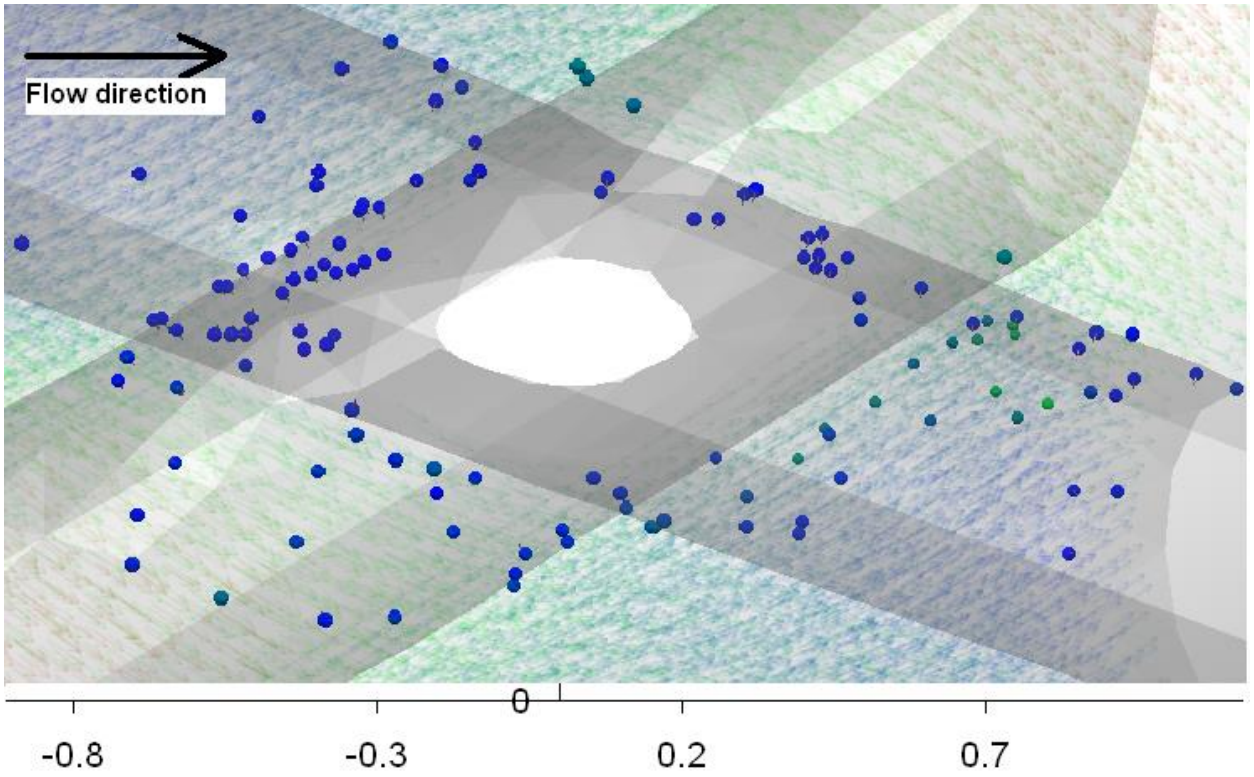

Figure.10: Deposition around Naltex 51-1 spacer joint (with distance scale in mm)

For configuration 51-1, Figure.9 and Figure.10 show there is a preferred deposition location in front of the spacer joint, which does not appear for configuration 51-2 or 51-3

where a constant deposition regardless of the position of the joint is exhibited. After the joint, 51-1 seems to display a similar deposition pattern as 51-2, Figure.11, and 51-3, Figure.12, meaning a uniform deposition along the filament.

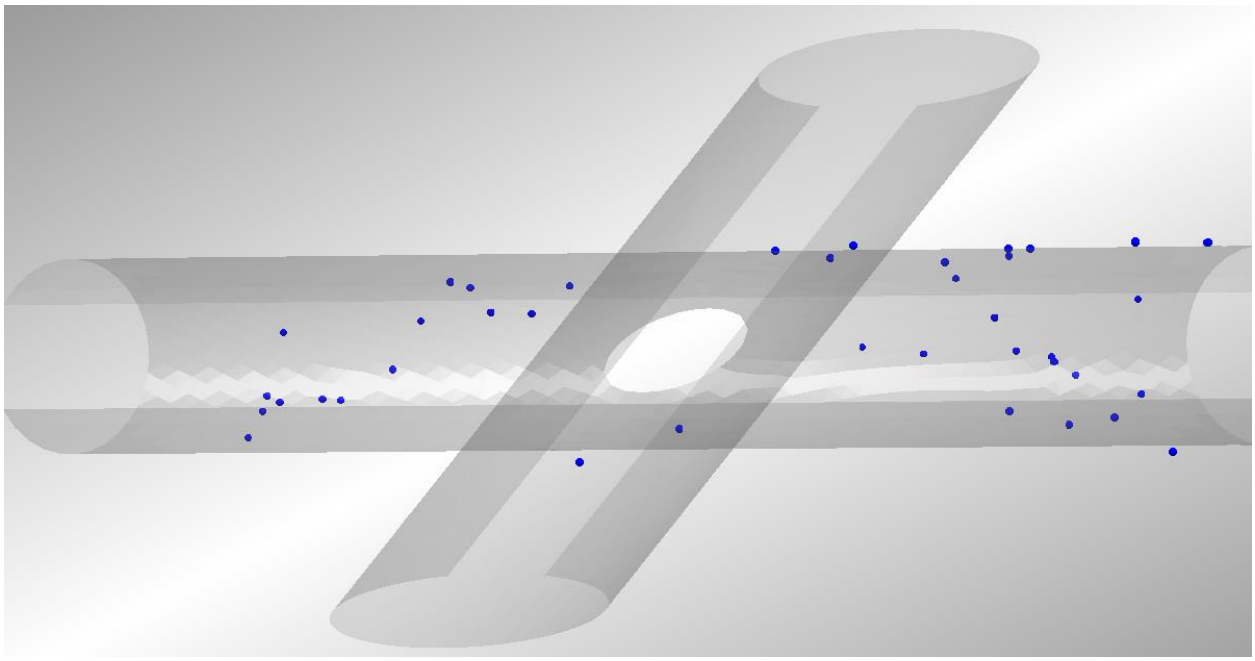

Figure.11: Deposition around Naltex 51-2 spacer joint

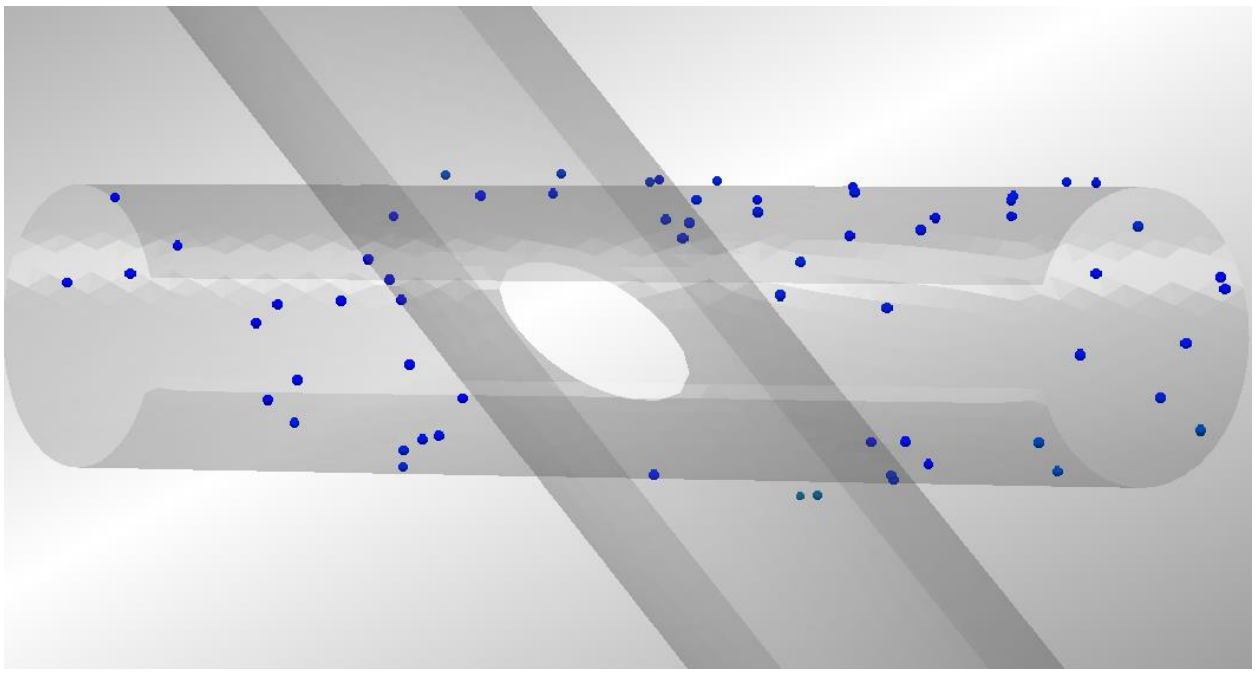

Figure.12: Deposition around Naltex 51-3 spacer joint

Although the spacer types are different, results show the same orientation sensitivity as experimental findings from Neal et al [20], who studied not the particle deposition on spacers but particle deposition in the gaps between them using square nets of equal sized

filaments. Results from the present work are in agreement with Neal's work; both results show that deposition numbers depend on spacer orientation. In the current study, with the filaments arranged symmetrically around the flow direction (Naltex 51-1), deposition occurred particularly at the filament junction, whilst in configurations with filaments parallel to the flow (51-2 and 51-3), deposition occurs across the entire longitudinal filament, parallel to flow. Neal also observed a zone of no deposition at the back of the transverse filament; this does not appear in our simulations. However, in Neal et al's work this applied when filaments are at a 90° angle, which is not the case for Naltex 51 spacer configuration used in this work.

Figure.13 displays the numbers of deposited particles around the spacer join with respect to time, the curve being derived from the number of particle-to-wall contacts in the zone displayed in red on the top part of the figure. It can be seen that after the first wall-to-particle contact in the red zone at around 0.3, Naltex 51-1 displays a much greater rate of deposition than the other two spacer geometries. This is attributable to the fact that for the simulations of Naltex 51-2 and 51-3, particles deposit upon impact and stay relatively immobile. On the other hand, for Naltex 51-1, particles depositing at any location on a spacer can still subsequently move and collect at the join, which makes the deposited particle count around the junction increase significantly with appear to increase at a higher rate time.

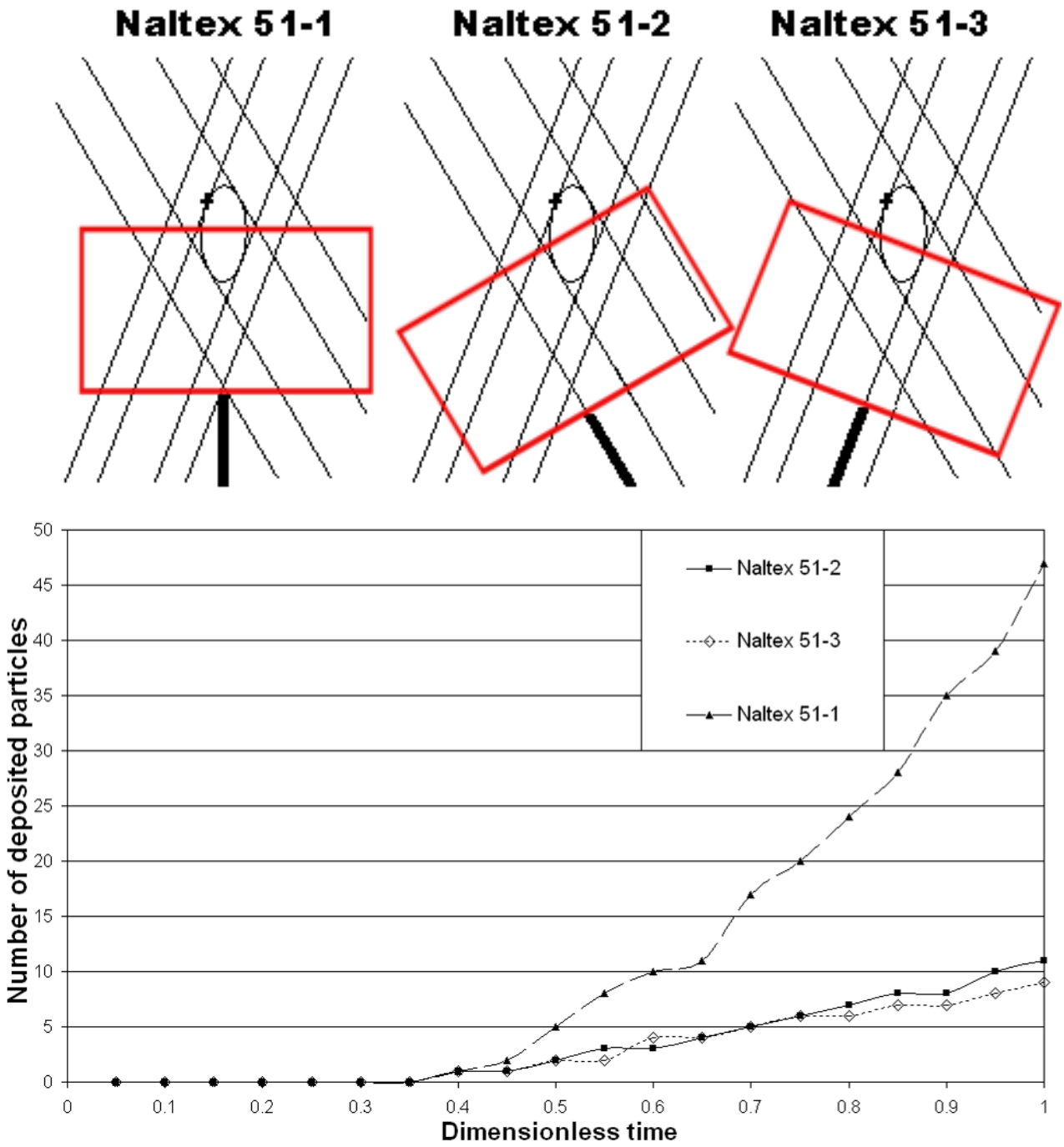

Figure.13: Evolution with time of deposited particles around spacer join

Vrouwenvelder's [39] experiments (Figure.14) shows deposition patterns similar to our simulation results. Where initial deposition occurring upstream of the spacer with a preferred deposition location at the spacer joint. Before, growth, propagation and colonisation occurs, which depend on nutrient availability, the initiation of bio-fouling is comparable to the particulate deposition simulated in the current study.

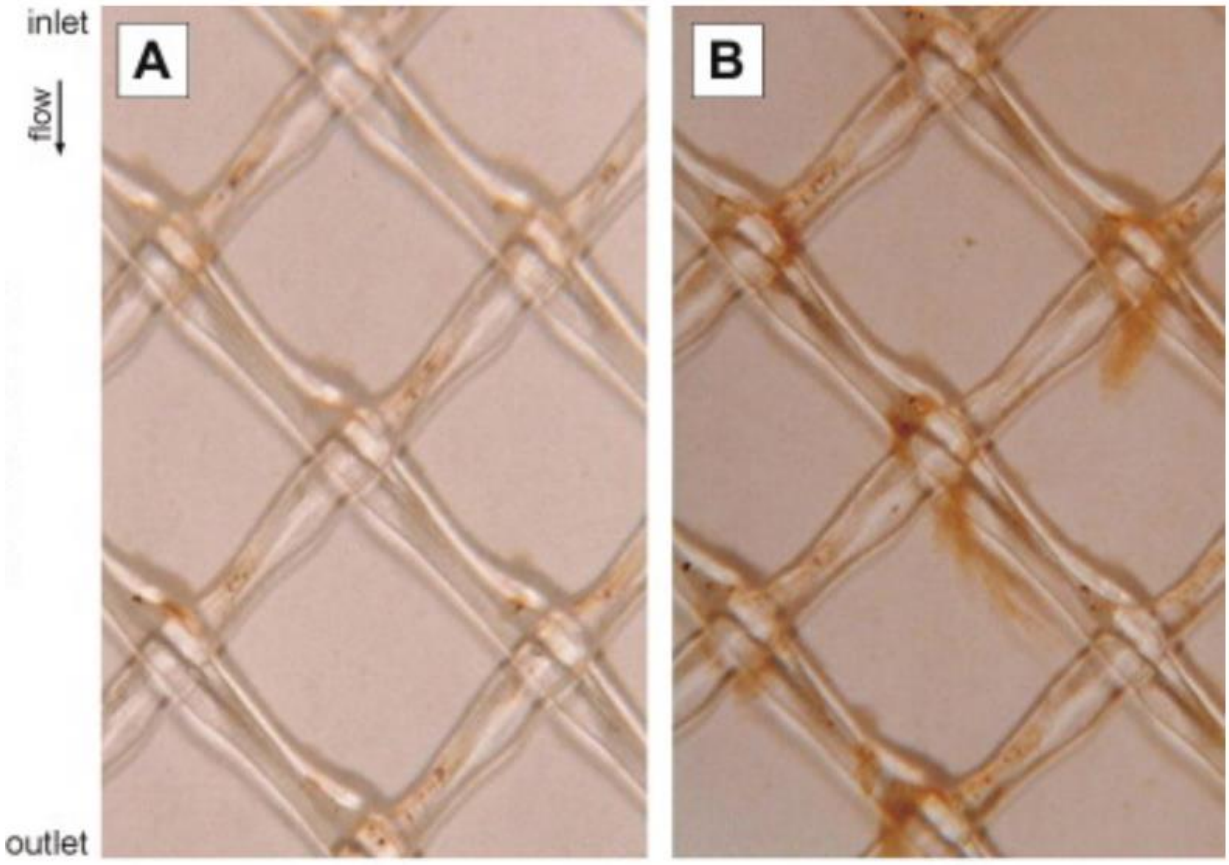

Figure.14: In-situ visual observations of the feed spacer and membrane without and with nutrient [39]

The observed fouling at the spacer junction agrees with some reports regarding microorganism deposition on spacers which state that the chance of attachment increases for decreasing values of shear stress around the obstacle [40, 41]. That would suggest increased deposition at regions of relatively low shear stress. The lowest shear is observed around the filament junction and away from spacer structures in between filament gaps, as shown in Figure.15.

It means that during initial deposition, adhesion simply occurs where the particles contact the filament, and tend to move in regions of low shear rate. The increase of biomass that occurs later compels the particles to shed in areas of lower shear strain (light green region between $-4s^{-1}$ and $2s^{-1}$ in Figure.15), toward the gaps between filaments.

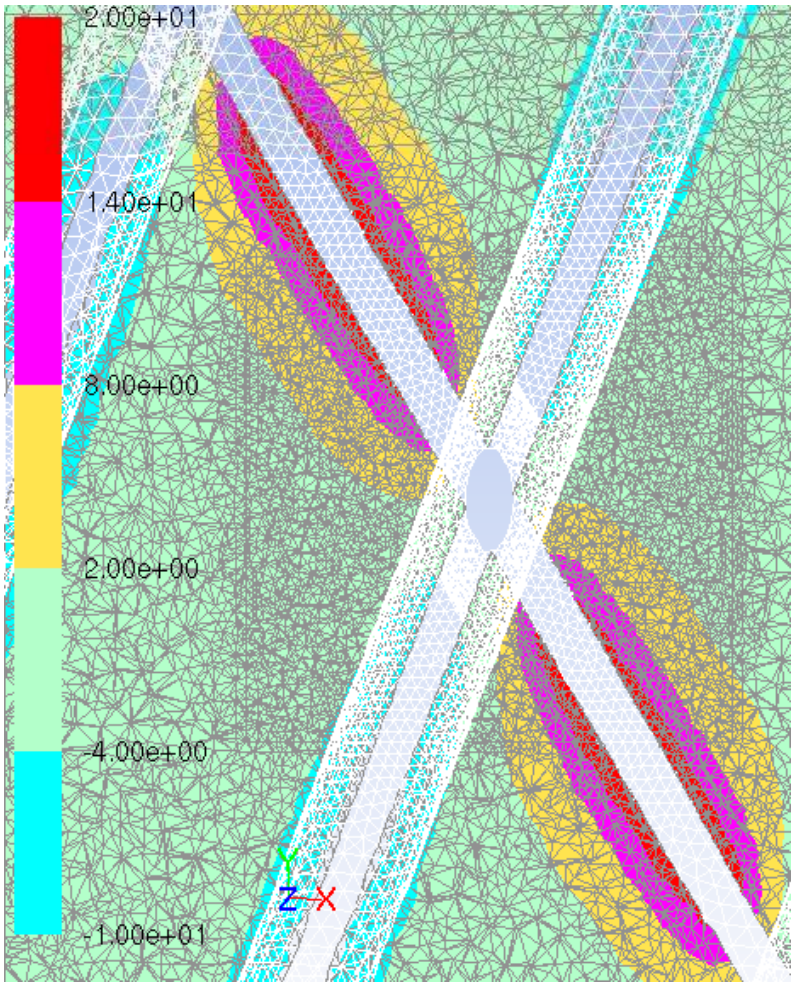

Figure.15: Shear rate contour around Naltex 51-1 spacer join

Under the flow, concentration and particle size conditions described in this work, very little particle-to-particle collision (Figure.16) could be observed. In the spacer feed channel, the ratio of particle volume to total volume was extremely small. Therefore, geometrical constraints were too low to induce bulk or surface cluster formation. Figure.16 shows a linear increase of inter-particle collision up to 0.45 of the total simulation time, which corresponds to the injected particles colliding amongst themselves up until they reach the filament junction. Then numbers drop as the un-deposited particles flow toward the outlet. That suggests that in these simulations, particle-to-particle collisions were not a significant factor for deposition

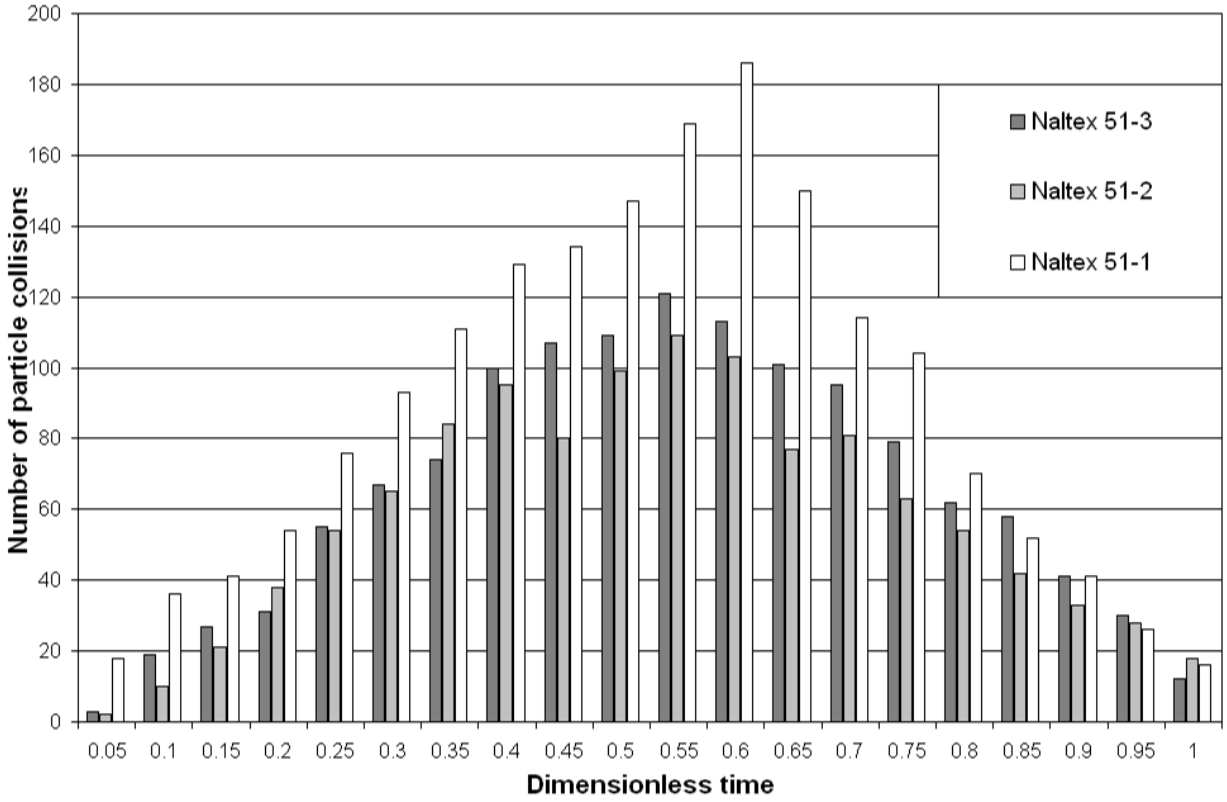

Figure.16: Comparison of particle collision around spacers

DEM-CFD method and EDEM post-processing capability allowed to follow the particle interactions with simulated structures and demonstrated that particle scale collisions were not significant for these simulations, but surface interaction models were still able to deposition pattern consistent with reported observations.

6 Conclusion

This work reports a study of incipient colloidal fouling around feed channel spacers typical of a spiral wound membrane, and how deposition morphology changes with spacer filament orientation. DEM has been used with a one way CFD coupling, in order to simulate the initial bio-film formation on the commercial membrane spacer Naltex 51. It has been found that initial deposition pattern appear in region of low shear stresses, which agrees with reported experiments, and simulations. A preferred deposition patterns that depends on spacer orientation is also predicted, and particle accumulation around Naltex51-1 filament junction was simulated, which is in coherence with reported observations.

References

1. Pak, A., et al., *CFD modeling of porous membranes.* Desalination, 2008. **222**(1-3): p. 482-488.
2. Kuznar, Z.A. and M. Elimelech, *Direct microscopic observation of particle deposition in porous media: Role of the secondary energy minimum.* Colloids and Surfaces A: Physicochemical and Engineering Aspects, 2007. **294**(1-3): p. 156-162.
3. Zimmerer, C.C. and V. Kottke, *Effects of spacer geometry on pressure drop, mass transfer, mixing behavior, and residence time distribution.* Desalination, 1996. **104**(1-2): p. 129-134.
4. Ngene, I.S., et al., *Particle deposition and biofilm formation on microstructured membranes.* Journal of Membrane Science. **364**(1â€“2): p. 43-51.
5. Da Costa, A.R., A.G. Fane, and D.E. Wiley, *Spacer characterization and pressure drop modelling in spacer-filled channels for ultrafiltration.* Journal of Membrane Science, 1994. **87**(1-2): p. 79-98.
6. Maharudrayya, S., S. Jayanti, and A.P. Deshpande, *Pressure losses in laminar flow through serpentine channels in fuel cell stacks.* Journal of Power Sources, 2004. **138**(1â€“2): p. 1-13.
7. Li, F., et al., *Optimization of commercial net spacers in spiral wound membrane modules.* Journal of Membrane Science, 2002. **208**(1-2): p. 289-302.
8. Li, F., et al., *Experimental validation of CFD mass transfer simulations in flat channels with non-woven net spacers.* Journal of Membrane Science, 2004. **232**(1-2): p. 19-30.
9. Karode, S.K. and A. Kumar, *Flow visualization through spacer filled channels by computational fluid dynamics I.: Pressure drop and shear rate calculations for flat sheet geometry.* Journal of Membrane Science, 2001. **193**(1): p. 69-84.
10. Wiley, D.E. and D.F. Fletcher, *Techniques for computational fluid dynamics modelling of flow in membrane channels.* Journal of Membrane Science, 2003. **211**(1): p. 127-137.
11. Shakaib, M., S.M.F. Hasani, and M. Mahmood, *CFD modeling for flow and mass transfer in spacer-obstructed membrane feed channels.* Journal of Membrane Science, 2009. **326**(2): p. 270-284.
12. Shakaib, M., S.M.F. Hasani, and M. Mahmood, *Study on the effects of spacer geometry in membrane feed channels using three-dimensional computational flow modeling.* Journal of Membrane Science, 2007. **297**(1-2): p. 74-89.
13. Wardeh, S. and H.P. Morvan, *CFD simulations of flow and concentration polarization in spacer-filled channels for application to water desalination.* Chemical Engineering Research and Design, 2008. **86**(10): p. 1107-1116.
14. Cao, Z., D.E. Wiley, and A.G. Fane, *CFD simulations of net-type turbulence promoters in a narrow channel.* Journal of Membrane Science, 2001. **185**(2): p. 157-176.
15. Ahmad, A.L. and K.K. Lau, *Impact of different spacer filaments geometries on 2D unsteady hydrodynamics and concentration polarization in spiral wound membrane channel.* Journal of Membrane Science, 2006. **286**(1-2): p. 77-92.
16. Ahmad, A.L., et al., *Integrated CFD simulation of concentration polarization in narrow membrane channel.* Computers & Chemical Engineering, 2005. **29**(10): p. 2087-2095.
17. Vrouwenvelder, J.S., et al., *A critical flux to avoid biofouling of spiral wound nanofiltration and reverse osmosis membranes: Fact or fiction?* Journal of Membrane Science, 2009. **326**(1): p. 36-44.
18. Bos, R., H.C. van der Mei, and H.J. Busscher, *Physico-chemistry of initial microbial adhesive interactions – its mechanisms and methods for study.* FEMS Microbiology Reviews, 1999. **23**(2): p. 179-230.

19. Schäfer, A.I., A.G. Fane, and T.D. Waite, *Nanofiltration: Principles and Application.* 2005.
20. Neal, P.R., et al., *The effect of filament orientation on critical flux and particle deposition in spacer-filled channels.* Journal of Membrane Science, 2003. **214**(2): p. 165-178.
21. Vrouwenvelder, J.S., et al., *Biofouling in spiral wound membrane systems: Three-dimensional CFD model based evaluation of experimental data.* Journal of Membrane Science. **346**(1): p. 71-85.
22. Bacchin, P., P. Aimar, and V. Sanchez, *Model for colloidal fouling of membranes.* AIChE Journal, 1995. **41**(2): p. 368-376.
23. Costerton, J.W., P.S. Stewart, and E.P. Greenberg, *Bacterial Biofilms: A Common Cause of Persistent Infections.* Science, 1999. **284**(5418): p. 1318-1322.
24. Metcalf and Eddy, *Wastewater Engineering : Treatment and reuse (4th Ed.)*
25. Li, Y.-L. and K.-L. Tung, *CFD simulation of fluid flow through spacer-filled membrane module: selecting suitable cell types for periodic boundary conditions.* Desalination, 2008. **233**(1â€“3): p. 351-358.
26. Ma, H., et al., *Hemispheres-in-Cell Geometry to Predict Colloid Deposition in Porous Media.* Environmental Science & Technology, 2009. **43**(22): p. 8573-8579.
27. A., L.H., Abh. theoret. Phys, 1907. **1 23**.
28. Brenner, H., *The slow motion of a sphere through a viscous fluid towards a plane surface.* Chemical Engineering Science, 1961. **16**(3-4): p. 242-251.
29. Nguyen, A.V. and G.M. Evans, *Exact and approximate expressions for resistance coefficients of a colloidal sphere approaching a solid surface at intermediate Reynolds numbers.* Applied Mathematical Modelling, 2007. **31**(4): p. 763-769.
30. Goldman, A.J., R.G. Cox, and H. Brenner, *Slow viscous motion of a sphere parallel to a plane wall--I Motion through a quiescent fluid.* Chemical Engineering Science, 1967. **22**(4): p. 637-651.
31. Goldman, A.J., R.G. Cox, and H. Brenner, *Slow viscous motion of a sphere parallel to a plane wall--II Couette flow.* Chemical Engineering Science, 1967. **22**(4): p. 653-660.
32. Ounis, H., G. Ahmadi, and J.B. McLaughlin, *Brownian diffusion of submicrometer particles in the viscous sublayer.* Journal of Colloid and Interface Science, 1991. **143**(1): p. 266-277.
33. Tien, C. and B.V. Ramarao, *The process of particle deposition in granular media: Description and formulation*, in *Granular Filtration of Aerosols and Hydrosols (Second Edition)*. 2007, Butterworth-Heinemann: Oxford. p. 337-403.
34. Overbeek, E.J.W.V.a.J.T.G., *Theory of the Stability of Lyophobic Colloids.* 1948.
35. Ma, H.L. and W.P. Johnson, *Colloid Retention in Porous Media of Various Porosities: Predictions by the Hemispheres-in-Cell Model.* Langmuir. **26**(3): p. 1680-1687.
36. Gregory, J., *Approximate expressions for retarded van der waals interaction.* Journal of Colloid and Interface Science, 1981. **83**(1): p. 138-145.
37. Rahimi, M., S.S. Madaeni, and K. Abbasi, *CFD modeling of permeate flux in cross-flow microfiltration membrane.* Journal of Membrane Science, 2005. **255**(1-2): p. 23-31.
38. Rajagopalan, R. and C. Tien, *Trajectory analysis of deep-bed filtration with the sphere-in-cell porous media model.* AIChE Journal, 1976. **22**(3): p. 523-533.
39. Vrouwenvelder, J.S., et al., *Biofouling of spiral-wound nanofiltration and reverse osmosis membranes: A feed spacer problem.* Water Research, 2009. **43**(3): p. 583-594.
40. Knutsen, J.S. and R.H. Davis, *Deposition of foulant particles during tangential flow filtration.* Journal of Membrane Science, 2006. **271**(1-2): p. 101-113.

41. Rahimi, M., et al., *CFD and experimental studies of fouling of a microfiltration membrane.* Chemical Engineering and Processing: Process Intensification, 2009. **48**(9): p. 1405-1413.